PAPER

Coupling of nonlinear shape memory polymer cantilever dynamics with focused ultrasound field

IOP Publishing Smart Materials and Structures
Smart Mater. Struct. **28** (2019) 055002 (14pp) https://doi.org/10.1088/1361-665X/ab0b71

Coupling of nonlinear shape memory polymer cantilever dynamics with focused ultrasound field

Aarushi Bhargava[1] **and Shima Shahab**[1,2]

[1] Department of Biomedical Engineering and Mechanics, Virginia Polytechnic Institute and State University, Blacksburg, VA 24061, United States of America
[2] Department of Mechanical Engineering, Virginia Polytechnic Institute and State University, Blacksburg, Va 24061, United States of America

E-mail: sshahab@vt.edu

Received 3 October 2018, revised 10 February 2019
Accepted for publication 28 February 2019
Published 29 March 2019

Abstract

Research has found significant potential for ultrasound actuation of shape memory polymers (SMPs) in several fields such as biomedical and electronic devices among others. Example applications range from controlled drug delivery containers to soft robotics and flexible electronics located in otherwise inaccessible places or hazardous environments, where direct external heating is not possible. SMPs can be manipulated into any temporary shape and later recover to their stress-free permanent shape when triggered with external stimuli such as heat. Focused ultrasound (FU) has the ability to induce localized heating and activate multiple intermediate shapes and achieve complete shape recovery in the polymer, non-invasively and remotely. In addition, FU has a superior capability for temporal and spatial control of shape recovery by adjusting sample size, ultrasound frequency, exposure time and intensity as well as the position of ultrasound focusing. In this paper, indirect actuation of the thermally-induced shape-memory effect of SMPs by FU is studied theoretically and experimentally with a focus on the acoustic field, medium, geometric and material properties. The changes in thermomechanical properties, during FU actuation, are studied through dynamic mechanical analyzer tests. Using these properties, an analytical acoustic-thermo-elastic dynamic model is developed to predict the shape memory response of a SMP cantilever beam, considering acoustic and geometric nonlinearities. The governing equations of motion are derived using reduced order modeling and solved by perturbation techniques. Having obtained an analytical expression for the shape recovery of the beam as a function of acoustic parameters, experimental validations for a cantilever SMP beam exposed to FU are performed. The model has the ability to successfully estimate the variation in the amount of shape recovery due to the change in source frequency of the transducer and peak acoustic pressure field inside SMP domain without the need of analyzing any intermediary acoustic/thermal/elastic behavior.

Supplementary material for this article is available online

Keywords: shape memory polymer, focused ultrasound actuation, nonlinear dynamics, nonlinear acoustic field

(Some figures may appear in colour only in the online journal)

1. Introduction

Shape memory polymers (SMPs) are an emerging class of smart materials which have gained significant attention in both industry and academic research due to their ability to memorize their permanent shape. This ability enables them to be manipulated into any temporary shape and later return to their stress-free permanent shape when triggered with different environmental

factors such as heat, light and magnetic field among others. Being polymers, they offer a wide variation in their mechanical properties in addition to being cheap, light-weight, biodegradable and easily process-able [1]. Last decade has observed an increasing use of SMPs in aerospace, biomedical, textile, structural and flexible electronic applications [2–4]. SMP-based controlled drug delivery devices, biodegradable sutures, catheters, cardiovascular stents actuated at body temperatures and microactuators are some of the emerging applications of SMPs in the biomedical industry [5–10].

The choice of environmental trigger for actuating SMPs is one of the key factors in attaining efficient shape recovery. Although, direct heat is one of the most commonly used trigger for shape memory effect, it is not always practical and safe, especially for heat-sensitive applications [11]. Consequently, other forms of actuating mechanisms such as irradiation (UV, IR and solar), magnetic field, electric current among others have come to forefront [12–17]. Chen *et al* [18] processed chitosan/PEG-based spiral coils as vascular stents which showed rapid shape recovery on hydration. Small *et al* [7, 19] studied the use of shape memory polyurethanes doped with light absorbing dyes for use as stents and foams. Sahoo *et al* [20, 21] used electric current to actuate shape memory polyurethanes coated with conductive polymer (PPy) and achieved 85%–90% of shape recovery. Thermomagnetically and electromagnetically induced shape memory effects can be achieved through fillers such as metal particles, iron (III) oxide [22, 23] and ferromagnetic particles [24]. Razzaq *et al* [25] actuated shape memory polyurethanes at lower field frequencies through micro-sized magnetite fillings. They achieved a considerable decrease in electrical resistivity and an increase in thermal conductivity with 40 vol% magnetite, and demonstrated a full shape recovery of SMP under magnetic field. Most of the triggers mentioned above either have no control over the shape memory response or require filler particles to induce shape memory behavior, which can compromise the structural/thermal integrity or biocompatibility of the polymer. A possible solution to overcome this challenge is the use of focused ultrasound (FU) as a safer, non-invasive remote trigger. An increased focus on ultrasound actuation is seen especially in biomedical applications where the need of a non-invasive and controllable trigger is of utmost importance [26–28]. FU enables selective, spatially and temporally controlled heating of SMP without the need of any filler particles. The underlying mechanism involves inducing heat generation due to viscous shearing oscillation of molecules under ultrasound exposure [29, 30], resulting in shape recovery. FU also offers significant advantage over other methods for actuation in applications requiring remote access. The limited literature of ultrasonic actuation of SMPs is mainly centered on proof-of-concept experiments demonstrating the feasibility of this method, lacking experimentally-validated modeling efforts for the resulting multiphysics problem that couples the domain acoustics with polymer dynamics. In this work, we present a coupled analytical and experimental multiphysics investigations for FU induced thermal actuation of a SMP cantilever, considering acoustic and weak geometric nonlinearities.

The use of thermally actuated SMPs in every application requires a comprehensive understanding of the thermo-mechanical process of shape recovery. Thus, the past two decades have observed several constitutive models to capture the shape memory behavior [31–34]. Liu *et al* [35] developed one of the first phenomenological constitutive models which considered SMPs as a mixture of two phases: the frozen phase (hard phase) and active phase (soft phase). The model describes the structural transformation of SMPs as being dependent on two internal state variables (the frozen phase volume fraction and stored strain). Several others improved this model by eliminating his model's assumptions [36–38]. This paper presents dynamic equations governing the motion of an ultrasound actuated SMP cantilever in heating, cooling and shape recovery stages, following the constitutive model developed by Liu *et al* [35] combined with acoustic-thermal equations. The FU nonlinear acoustic field and induced thermal energy are obtained using Khokhlov–Zabolotskaya–Kuznetsov (KZK) [39, 40] and Penne's Bioheat [41] equations, respectively [42]. The behavior of temperature dependent mechanical properties of SMP is studied using dynamic mechanical analyzer (DMA) tests. A model is built to predict the shape memory response of a SMP based cantilever beam subjected to pure bending and the governing equations of motion for all the stages of the shape recovery process are derived, using reduced order mathematical modeling. An analytical dynamic solution is then developed using perturbation techniques for a weakly geometric nonlinear SMP cantilever to estimate the acoustically driven recovery of the beam. The experimentally-validated analytical solution is then used to characterize the acoustic parameters and their effects on ultrasound induced shape recovery of the beam. The scope of this work encompasses all applications of thermally actuated SMPs requiring shape recovery such as SMP based switches and drug delivery containers among others. In section 2, we develop the theoretical background and acoustic-thermo-elastic model for an ultrasound-SMP actuation system. Experimental results and model validation are presented in section 3. A summary and conclusions are presented in section 4.

2. Theory

In order to understand the nonlinear dynamics of FU induced thermal actuation of SMPs, a robust model which predicts the acoustic and thermal fields and subsequent shape recovery is essential. The model is divided into three interconnected parts. The first part uses KZK equation [39, 40] to estimate the focused acoustic pressure field inside an SMP submerged in water [30]. The equation is numerically solved in a hybrid time-frequency domain taking into account the effects of absorption, diffraction and nonlinearity in the medium. The second part solves Penne's Bioheat equation [41] to calculate the FU induced temperature rise inside the polymer. The third part predicts the shape recovery of SMP using a constitutive model developed by Liu *et al* [35]. The dynamic response of a SMP cantilever beam is derived using reduced order mathematical modeling and solved using perturbation techniques. The advantages of such techniques over numerical methods is the flexibility to study the

characteristics of the nonlinear response and determine the effect of various acoustic and SMP geometric and material parameters individually on the shape recovery effect. The governing equations of motion are developed using Generalized Hamilton's Principle [43], assuming an SMP filament as an Euler–Bernoulli cantilever beam. We use Galerkin weighted residual method [43] to convert the partial differential governing equations into n modal ordinary differential equations. The method of multiple scales [44] is then used to develop an analytical solution to predict the shape recovery of SMP as a function of acoustic and thermal parameters.

2.1. Multiphysics acoustic-thermal-elastic modeling

KZK equation is used to predict the nonlinear FU generated acoustic pressure field in SMP and fluid domains. The non-dimensional form of the equation is [40]

$$\frac{\partial^2 \overline{p}}{\partial \tau \partial \overline{z}} = \left(\frac{1}{4G}\nabla^2_{\overline{r}} + \overline{A}\frac{\partial^3}{\partial \tau^3}\right)\overline{p} + \frac{\overline{B}}{2}\frac{\partial^2 \overline{p}^2}{\partial \tau^2}, \tag{1}$$

where the non-dimensional pressure, $\overline{p}$, is given as $\overline{p} = p/p_0$. Here, p is the pressure at the observation point and p_0 is the characteristic source pressure. The non-dimensional form of propagation distance, $\overline{z}$ is given as $\overline{z} = z/D$ where D is the focal distance and z is the axial distance in the direction of wave propagation, Z. The retarded time is given as $\tau = f_0(t - z/c)$ where f_0 is the source frequency, t is time and c is the speed of sound in the acoustic medium. The parameter $\nabla^2_{\overline{r}} = (\partial^2/\partial \overline{r}^2 + \partial/\overline{r}\partial \overline{r})$ is the non-dimensional form of the Laplacian where $\overline{r} = r/a$ is the dimensionless form of the radial distance r along the radial coordinate axis, R, and a is the radius of the transducer. The parameters $\overline{A}$, G and $\overline{B}$ represent the attenuation, gain and nonlinearity of the medium respectively. A detailed explanation of the equation and solving technique is given by Bhargava *et al* [30]. This acoustic framework can also be used for ultrasonic energy transfer systems using FU sources [45–48]. The calculated pressure field is then used as an input to Penne's Bioheat equation [41] which predicts the thermal field generated due to viscous shearing exerted by focused ultrasound waves inside the polymer. The equation is given as

$$\rho_m C_{hm}\frac{\partial T}{\partial t} = \kappa \nabla^2 T + H, \tag{2}$$

where T is the temperature of the medium at the observation point. The parameters ρ_m, C_{hm} and κ are the density, specific heat capacity, and thermal conductivity of the medium respectively. In equation (2), the accumulated heat H is due to absorption of the pressure field in the polymer and is given as $H = (1/\rho_m c)\sum_{n=1}^{k} \mathrm{Re}[\overline{a}_n]|p_n|$ for up to k harmonics. Here, Re[ ] denotes the real part of a quantity. The parameter $\overline{a}_n$ accounts for absorption and dispersion of the propagating wave in the medium and is a complex number. The real part of this term represents the absorption coefficient at kth harmonic. As a result of viscous shearing exerted by ultrasound waves due to the absorption of the pressure field of kth harmonic, energy is released in the form of heat, leading to temperature rise in the polymer filament.

The temperature rise in the polymer results in a mechanical response which subsequently causes shape recovery of the polymer. A constitutive model developed by Liu *et al* [35] is used to capture the thermomechanical response. The model uses the glass transition temperature, T_g, to define the relationship between the final recoverable stress and strain. The shape recovery process involves four stages with the first stage as the loading stage where the polymer is heated above its T_g and deformed to a temporary shape by an external force. The second stage is cooling the polymer below its T_g to fix the temporary deformed shape. The third stage is unloading of the external forces and the fourth stage is re-heating the polymer to attain shape recovery. Liu's [35] model quantifies the storage and release of entropic deformation in the form of 'frozen' strains which are equal to the strains in the pre-deformed body at the end of loading stage, in our study. During cooling, the pre-deformed strains freeze in the polymer and are released upon ultrasound actuation and the body returns to its original shape. The model is derived using the evolution of storage strains during the cooling process only, but is assumed to hold true for both cooling and re-heating stages of the shape recovery process under monotonous decreasing and increasing temperature profiles, respectively. The model has shown reasonable agreements with experiments for both these stages [35]. However, in case of repeated cooling/heating intermediary cycles, a net cooling history needs to be incorporated in the model to account for any partial storage/release of stored strains [49, 50]. Since, in this work, temperature profiles of cooling and heating due to ultrasound actuation are strictly decreasing and increasing respectively, Liu's model [35] is used. The model defines the 1D constitutive equation and temperature derivative of stored strain for the SMP, as equations (3) and (4), respectively [35].

$$\sigma = \frac{\varepsilon - \varepsilon_s - \int_{T_h}^{T} \alpha dT}{\dfrac{\phi_f}{E_i} + \dfrac{1-\phi_f}{E_e}} = E\left(\varepsilon - \varepsilon_s - \int_{T_h}^{T} \alpha dT\right) \tag{3}$$

$$\frac{d\varepsilon_s}{dT} = \frac{E}{E_e}\left(\varepsilon - \varepsilon_s - \int_{T_h}^{T} \alpha dT\right)\left(\frac{d\phi_f}{dT}\right), \tag{4}$$

where ε is the total strain and σ is the total stress in the body. The parameters ε_s, α and T_h represent the temperature, T, dependent storage strain, thermal expansion coefficient and maximum temperature up to which SMP is heated in loading stage before deformation, respectively. The frozen fraction ϕ_f represents the fraction of the volume in the frozen (stiffer) phase and is given as $\phi_f = 1 - [1 + c_f(T_h - T)^n]^{-1}$, where c_f and n are variables which can be experimentally found by curve fitting method. The Young's modulus E is related to temperature by the relation, $E = [(\phi_f/E_i) + (1 - \phi_f/E_e)]^{-1}$ where E_i is the modulus of the internal energetic deformation and E_e is the modulus of the entropic deformation calculated using the formulae, $E_e = 3NkT$. The parameters N and k denote the cross-link density and Boltzmann's constant ($k = 1.38 \times 10^{-23}$ Nm K^{-1}) respectively. The model given by equations (3) and (4) exhibits a linear stress-strain relationship and assumes rubbery elasticity to hold true as long as

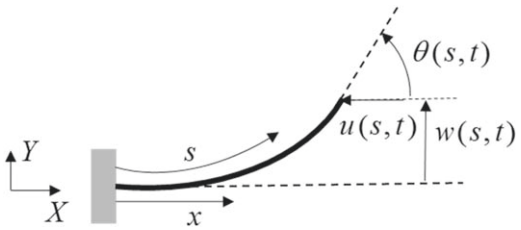

Figure 1. Schematic of deformation of cantilever beam in pure bending due to end point force (positive Y direction) at the free end. The dashed line represents the original position of the beam. X and Y are the global coordinates of the system.

the strains and cross-linking density fall in the domain of small-moderate (40%–50%) [35, 51–56]. Note that the strains in this work are not small, but lie in the domain such that rubbery linear elasticity assumption gives good approximation with experimental data.

To develop a comprehensive understanding of the dynamic response of SMP during shape recovery process, we develop governing equations of motions for each stage of shape recovery process for an Euler–Bernoulli SMP cantilever beam using Generalized Hamilton's principle. We then solve these equations using Galerkin's weighted residual method and method of multiple scales and validate the results with experiments and numerical solution of the governing equation. The main aim is to express the dynamic shape recovery of the SMP cantilever as a function of the FU parameters through an analytical expression.

2.2. Nonlinear SMP cantilever dynamics: loading, cooling, shape fixation and shape recovery

A SMP cantilever beam with length l, width b and thickness h is shown in figure 1. The beam's response is derived under the assumptions of Euler–Bernoulli beam which considers the beam to have a higher length to thickness ratio, such that the rotational effects and angular distortion of the differential element are ignored. Consequently, shear effects in beams with large aspect ratio are neglected. However, they can be incorporated to obtain better approximation. In this work, for simplification, shear effects are neglected for a cantilever beam with large aspect ratio in order to obtain an analytical solution of the complicated dynamics of acoustic-thermoelastic coupling in SMPs with sufficient accuracy (shown in section 3). Linear elasticity is assumed for the range of strains $\leqslant$40%. The beam is subjected to pure bending such that deflections are large but curvature remains small, i.e. curvature is proportional to bending moment. In this work, we used the nonlinear 2D Euler–Bernoulli beam theory with allowance for damping, following the theory developed by Nayfeh and Pai [57]. The condition of inextensibility is assumed for simplification and to obtain and analytical solution with good approximation [58].

The generalized Hamilton's principle is stated as

$$\int_{t_1}^{t_2} (\delta T_E - \delta U_E + \delta W_{nc}) dt = 0, \tag{5}$$

where δT_E, δU_E and δW_{nc} are the variations in kinetic energy, potential energy and the work done by non-conservative forces. The potential energy of a cantilever beam in pure bending with no gravitational effects, is given by

$$U_E = \frac{1}{2}\int_V E y^2 \gamma^2 dA ds = \frac{1}{2}\int_0^l EI\gamma^2 ds, \tag{6}$$

where γ is the curvature denoted by $\gamma = \partial\theta(s,t)/\partial s$ (inextensible), $\theta(s)$ is the angle of the perpendicular to the cross-section, dA, of the beam with the horizontal axis X, s is the curvilinear coordinate along the length of the beam and E is the Young's modulus. The parameter $I = \int_A y^2 dA$ is the area moment of inertia of the beam where y is the distance from the neutral axis. By defining w as the vertical deflection of the beam (figure 1) and realizing that $\theta(s,t) = \sin^{-1}[w'(s,t)] = w'(s,t) + w'(s,t)^3/6$, the potential energy till fourth order i.e. $O([\,]^{n>4}) = 0$, can be expressed as $U_E = \frac{1}{2}EI\int_0^l (w''(s,t)^2 + w'(s,t)^2 w''(s,t)^2) ds$. The kinetic energy T_E is given by

$$T_E = \frac{1}{2}\rho A\int_0^l (\dot{u}(s,t)^2 + \dot{w}(s,t)^2) ds + \frac{1}{2}\int_0^l \rho I\dot{\theta}(s,t)^2 ds, \tag{7}$$

where ρ is the density of the SMP, A is the area, u is the horizontal displacement of the beam and $\dot{(\cdot)}$ is the time derivative of a quantity. The second term on the right hand side of equation (7) accounts for rotational inertia effect and will be ignored in the rest of this study due to its negligible contribution. From geometry (figure 1), using the relation $\cos[\theta(s,t)] = 1 - u'(s,t)$, expressing it in terms of w and substituting in equation (7), gives the expression for kinetic energy as $T_E = \frac{1}{2}\rho A \int_0^l \left(\left(\int_0^s (w')(s,t)\dot{w}'(s,t) + \frac{w'(s,t)^3\dot{w}'(s,t)}{2} d\xi\right)^2 + \dot{w}(s,t)^2\right) ds$. The virtual work done by non-conservative forces is

$$\delta W_{nc} = \frac{1}{2}\int_0^l EI\delta(\gamma_s(s,t)^2) ds - \int_0^l F\delta w(s,t) ds - \int_0^l d_1\dot{w}(s,t)\delta w(s,t) ds, \tag{8}$$

where F is a distributed external force per unit length and damping coefficient is denoted by d_1. The first term in equation (8) is a contribution of the energy due to frozen strains, $\varepsilon_s(s,T)$ obtained from equation (4) and thermal strains, $\varepsilon_T(t)$. This approach arises from the understanding that all mechanical, frozen and thermal strains contribute to the overall stress of the system through the relation given by equation (3). Therefore, the energy contribution due to this stress can be expressed as the energy contribution from each of the mechanical, frozen and thermal strains individually, as the stress-strain relation is linear [51]. To accomplish this, the mechanical strains are assumed to contribute to the potential energy of the system (similar to any beam system) and the rest of the strains are assumed to contribute to the external

work done. Since ε_s is a function of spatial variable s and temperature T, which is a function of time t from equation (2), ε_s can be represented as, $\varepsilon_s(s, t)$. The parameter $\gamma_s(s, t)$ in the first term of equation (8) is the curvature associated with $\varepsilon_s(s, t)$ and $\varepsilon_T(t)$, and is expressed as $\gamma_s(s, t) = w_s''(s, t) + w_s'(s, t)^2 w_s''(s, t)/2+$ higher order terms. Taking the variation of equations (6) and (7) and substituting them in equation (5) along with equation (8) yields the governing equation of motion as

$$\begin{aligned}&\rho A\left(\left(\frac{w'(s,t)}{2}\int_s^l\int_0^s \frac{\partial^2 w'(s,t)^2}{\partial t^2}d\xi ds\right)' - \ddot{w}(s,t)\right)\\&- EI(w''''(s,t) - w_s''''(s,t))\\&- EI((w'(s,t)(w'(s,t)w''(s,t))')'\\&- (w_s'(s,t)(w_s'(s,t)w_s''(s,t))')') - d_1\dot{w}(s,t) - F = 0\end{aligned} \tag{9}$$

with geometric boundary conditions at $s = 0$ as

$$w(s,t)|_{s=0} = 0 \tag{10}$$

$$w'(s,t)|_{s=0} = 0. \tag{11}$$

And natural boundary conditions from moment and shear at $s = l$ as

$$\begin{aligned}&w''(s,t) + w'^2(s,t)w''(s,t) - w_s''(s,t)\\&\quad - w_s'^2(s,t)w_s''(s,t)\Big|_{s=l}\\&= 0\end{aligned} \tag{12}$$

$$\begin{aligned}&w'''(s,t) + w'''(s,t)w'(s,t)^2 + w'(s,t)w''(s,t)^2\\&-w_s'''(s,t) - w'''_s(s,t)w_s'(s,t)^2 - w_s'(s,t)w_s''(s,t)^2\Big|_{s=l} = 0.\end{aligned} \tag{13}$$

The time dependency in equation of motion arises during the shape recovery stage. This time dependency is due to the rise in temperature with time during ultrasound actuation, equation (2). Since stored strains are a function of temperature, equation (4), the release of storage strains become time dependent during shape recovery stage. As the material is elastic for the range of strains $\leqslant$40% [51], the stored strains are instantaneously released when the temperature reaches the glass transition temperature.

2.2.1. Loading and cooling. In this stage, the SMP is heated to an elevated temperature T_h such that the SMP is in rubbery phase and the frozen fraction is zero. After heating, SMP is deformed to a temporary shape in the upward direction by a force P_y applied at the tip end (figure 1). Due to static loading, time derivative terms are zero and with no contribution of frozen energy, the terms with variable w_s are zero in equations (9)–(13). Equation (9) for this stage in terms of $\theta(s)$ with $F = \int_0^l P_y\delta^*(s-l)ds$ becomes [59]

$$E_h I\theta''(s) + P_y\cos[\theta(s)] = 0 \tag{14}$$

with boundary conditions $\theta(0) = 0$ and $\theta'(l) = 0$. In equation (14), E_h is the elastic modulus at T_h. The equation of motion for static loading, equation (14) is expressed in $\theta(s)$ due to ease of solving as compared to solving in terms of transverse displacement $w(s)$. A detailed derivation of this equation is given in [60]. Wang *et al* [61] derived the solution of equation (14) for large deflections using homotopy analysis method. In this study, we used a similar approach to estimate the deflection of the beam in the loading stage. The strains at the end of this stage are denoted by ε_{pre}.

The SMP cantilever beam is cooled to a temperature below T_g under the pre-strain constraint [35] i.e. maintaining the deformed shape. This results in freezing of the thermally reversible molecular chains and the deformation history is stored in the form of frozen energy which can be released by heating the SMP again.

2.2.2. Fixation and shape recovery. After cooling, the external forcing is removed and the deformed shape of the cantilever beam is fixed. Setting $\varepsilon = \varepsilon_{pre}$ in equation (4) and using equation (2), $\varepsilon_s(s, t)$ is obtained which leads to $\gamma_s(s, t)$ in equation (8). Equations (9)–(13) are discretized using $w(s, t) = \sum_{i=1}^{\infty}\varphi_i(s)\eta_i(t)$ where $\varphi_i(s)$ represents mode shape associated with ith natural frequency, $\eta_i(t)$ is the ith modal coordinate. Setting external force distribution $F = 0$, applying Galerkin's weighted residual method to equation (9) [57] and considering only one mode, equation of motion for shape recovery is,

$$\psi\eta(\eta\ddot{\eta} + \dot{\eta}^2) + \ddot{\eta} + \eta\omega^2 + 2\mu\dot{\eta} + \bar{\zeta}\eta^3 - \xi(t) - \bar{\xi}(t) = 0, \tag{15}$$

where $\psi = \rho A\int_0^l \varphi'^2\left(\int_s^l\int_0^s \varphi'^2 d\xi dh\right)ds$, $\mu = \frac{d_1}{2}\int_0^l \varphi^2 ds$, $\bar{\zeta} = EI\int_0^l (\varphi'^2)'(\varphi'\varphi'')ds$, $\xi(t) = EI\int_0^l \varphi''w''_s(s,t)ds$, $\bar{\xi}(t) = EI\int_0^l (\varphi' w_s'(s,t))'(w_s'(s,t)w_s'(s,t))ds$ and ω is the natural circular frequency (rad/s) such that $\omega^2 = \beta^4 EI/\rho A$ with β being the eigen value obtained from the characteristic equation of the undamped and unforced linear system, obtained by reducing equations (9)–(13) [43].

Here $\xi(t)$ and $\bar{\xi}(t)$ are functions of w_s, which change with time as the SMP is heated. For fixation, the beam is below the T_g and is in static position when the external forces are removed. It is assumed that the entire polymer has transformed to glassy state and has completely stored the energy due to strains developed in loading stage. Therefore, the equation for the deformation of the beam in this stage is obtained by setting time derivative terms to zero and taking $\xi(t)$ and $\bar{\xi}(t)$ at time $t = 0$ in equation (15). The governing equation thus becomes,

$$\eta\omega^2 + \bar{\zeta}\eta^3 - \xi(0) - \bar{\xi}(0) = 0. \tag{16}$$

The above stated approach gives an approximate solution for these shape recovery stages, however, the error is minimized by using Galerkin's weighted residual method [62].

2.3. Solution approach using method of multiple scales

During ultrasound actuation, the thermal field developed inside SMP leads to shape recovery due to release of temperature dependent frozen energy. Equation (15) represents the equation of motion in this stage where time t is the duration of ultrasound actuation. To obtain the magnitude of the shape recovery, method of multiple scales [44, 63] is used to find an approximate solution of equation (15) in case of weak nonlinearities. A technique similar to Meesala *et al* [64] is followed where a bookkeeping parameter, $\tilde{\varepsilon}$ is introduced which signifies the effect of each term in equation (15) on the final response. Equation (15) is re-written as

$$\tilde{\varepsilon}\psi\eta(\eta\ddot{\eta}+\dot{\eta}^2)+\ddot{\eta}+\eta\omega^2+2\tilde{\varepsilon}\mu\dot{\eta}+\tilde{\varepsilon}\overline{\zeta}\eta^3-\xi(t)-\overline{\xi}(t)=0, \tag{17}$$

where η depends on t and $\tilde{\varepsilon}$. During heating, the temperature dependent elastic modulus E changes with time, since $T=T(t)$. To account for this variation in E, the process of re-heating in fourth stage is divided into multiple stages of small time intervals, with each stage having a constant modulus. This multi-stage division is necessary to have constant coefficients of nonlinearities in equation (17) and to derive an approximate analytical solution. Equation (17) is thus applied to each of these stages to obtain the response of the beam till the nonlinear terms become negligible and the response can be accurately predicted by linear equation

$$\ddot{\eta}+\eta\omega^2+2\mu\dot{\eta}-\xi(t)-\overline{\xi}(t)=0. \tag{18}$$

An approximate solution for equation (17) is expressed in the form of power series in η given by

$$\eta(t;\tilde{\varepsilon})=\eta_0(t)+\tilde{\varepsilon}\eta_1(t)+\tilde{\varepsilon}^2\eta_2(t)+\text{higher order terms}. \tag{19}$$

Retaining up to $O(\tilde{\varepsilon}^1)$ terms, the dependence of η on t and $\tilde{\varepsilon}$ occurs on different time scales, T_0 and T_1 such that $T_n=\tilde{\varepsilon}^n t$ for $n=0, 1$. Using chain rule, the differentiation terms with respect to t can be expressed as $\frac{D}{Dt}=\frac{\partial}{\partial T_0}+\tilde{\varepsilon}\frac{\partial}{\partial T_1}\equiv D_0+\tilde{\varepsilon}D_1$ and $\frac{D^2}{Dt^2}=\frac{\partial^2}{\partial {T_0}^2}+2\tilde{\varepsilon}\frac{\partial^2}{\partial T_0\partial T_1}+\tilde{\varepsilon}^2\frac{\partial^2}{\partial {T_1}^2}\equiv {D_0}^2+2\tilde{\varepsilon}D_0D_1+\tilde{\varepsilon}^2{D_1}^2$. The solution form, equation (19) now becomes a function of new time scales, given by

$$\eta(t;\tilde{\varepsilon})=\eta_0(T_0,T_1)+\tilde{\varepsilon}\eta_1(T_0,T_1)+\tilde{\varepsilon}^2\eta_2(T_0,T_1)+\text{higher order terms}. \tag{20}$$

Expressing equation (17) using equation (20), and retaining up to $O(\tilde{\varepsilon}^1)$ terms, equations for each order of $\tilde{\varepsilon}$ are given as,

$$O(\tilde{\varepsilon}^0):\ \omega^2\eta_0+{D_0}^2\eta_0=-\overline{F}, \tag{21}$$

where $\overline{F}$ is used to denote combined stored energy effect, $\overline{F}=-\xi(T_0)-\overline{\xi}(T_0)$.

$$O(\tilde{\varepsilon}^1):\ {D_0}^2\eta_1+\eta_1\omega^2=\overline{\zeta}{\eta_0}^3-\psi\eta_0(D_0\eta_0)^2-2D_0D_1\eta_0-\psi{\eta_0}^2{D_0}^2\eta_0-2\mu D_0\eta_0. \tag{22}$$

The solution of equation (21) is of the form

$$\eta_0=\frac{-\overline{F}}{\omega^2}+e^{i\omega T_0}A(T_1)+e^{-i\omega T_0}\overline{A}(T_1), \tag{23}$$

where the second and the third terms on the right hand side of equation (23) are complex conjugates and i an denotes imaginary number. Using equation (23) in equation (22),

$$\begin{aligned}{D_0}^2\eta_1+\eta_1\omega^2=&-\frac{\overline{F}^3\overline{\zeta}}{\omega^6}+\frac{3e^{i\omega T_0}\overline{F}^2\overline{\zeta}A}{\omega^4}+\frac{e^{i\omega T_0}\overline{F}^2\psi A}{\omega^2}\\&-3e^{2i\omega T_0}\overline{F}\psi A^2-\frac{3e^{2i\omega T_0}\overline{F}\overline{\zeta}A^2}{\omega^2}\\&+e^{3i\omega T_0}\overline{\zeta}A^3+2e^{3i\omega T_0}\omega^2\psi A^3\\&-2\psi\overline{F}A\overline{A}-\frac{6\overline{F}\overline{\zeta}A\overline{A}}{\omega^2}+3e^{i\omega T_0}\overline{\zeta}A^2\overline{A}\\&+2e^{i\omega T_0}\omega^2\psi A^2\overline{A}-2ie^{i\omega T_0}\omega A\mu\\&-2ie^{i\omega T_0}\omega D_1A\\&+\text{complex conjugates}.\end{aligned} \tag{24}$$

For a bounded solution, secular terms should be eliminated and are therefore set to zero.

$$\begin{aligned}&-\frac{3e^{i\omega T_0}\overline{F}^2\overline{\zeta}A}{\omega^4}-\frac{e^{i\omega T_0}\overline{F}^2\psi A}{\omega^2}-3e^{i\omega T_0}\overline{\zeta}A^2\overline{A}\\&-2e^{i\omega T_0}\omega^2\psi A^2\overline{A}+2ie^{i\omega T_0}\omega A\mu+2ie^{i\omega T_0}\omega D_1A=0\end{aligned} \tag{25}$$

$$\begin{aligned}&-\frac{3e^{-i\omega T_0}\overline{F}^2\overline{\zeta}\overline{A}}{\omega^4}-\frac{e^{-i\omega T_0}\overline{F}^2\psi\overline{A}}{\omega^2}-3e^{-i\omega T_0}\overline{\zeta}\overline{A}^2A\\&-2e^{-i\omega T_0}\omega^2\psi\overline{A}^2A-2ie^{-i\omega T_0}\omega\overline{A}\mu-2ie^{-i\omega T_0}\omega D_1\overline{A}=0\end{aligned} \tag{26}$$

Equations (25) and (26) are complex conjugates and satisfying one consequently satisfies the other. Substituting $\frac{1}{2}ae^{i\beta}$ for A and $\frac{1}{2}ae^{-i\beta}$ for $\overline{A}$ and making real and imaginary terms equal to zero, we obtain

$$\begin{aligned}&a=A_0e^{-T_1\mu}\text{ and }\beta\\&=\frac{-4\overline{F}^2(3\overline{\zeta}+\psi\omega^2)T_1+\frac{e^{-2T_1\mu}\omega^4(3\overline{\zeta}+2\psi\omega^2){A_0}^2}{2\mu}}{8\omega^5}+\beta_0\end{aligned} \tag{27}$$

where A_0 and β_0 are constants and depend on initial conditions of the SMP system. Eliminating secular terms from equation (24), the solution is derived as

$$\begin{aligned}\eta_1=&-\frac{\overline{F}^3\overline{\zeta}}{\omega^8}+\frac{e^{2i\omega T_0}\overline{F}\overline{\zeta}A^2}{\omega^4}+\frac{e^{2i\omega T_0}\overline{F}\psi A^2}{\omega^2}\\&-\frac{1}{4}e^{3i\omega T_0}\psi A^3-\frac{e^{3i\omega T_0}\overline{\zeta}A^3}{8\omega^2}-\frac{6\overline{F}\overline{\zeta}A\overline{A}}{\omega^4}\\&-\frac{2\overline{F}\psi A\overline{A}}{\omega^2}+Ae^{i\omega T_0}+\text{complex conjugates}.\end{aligned} \tag{28}$$

Substituting equations (23), (27) and (28) in equation (19) gives the approximate solution of $\eta(t)$ upto O($\tilde{\varepsilon}^1$). We use this approximate solution to calculate the shape recovery of the beam for multiple stages and verify with numerical solution of equation (15).

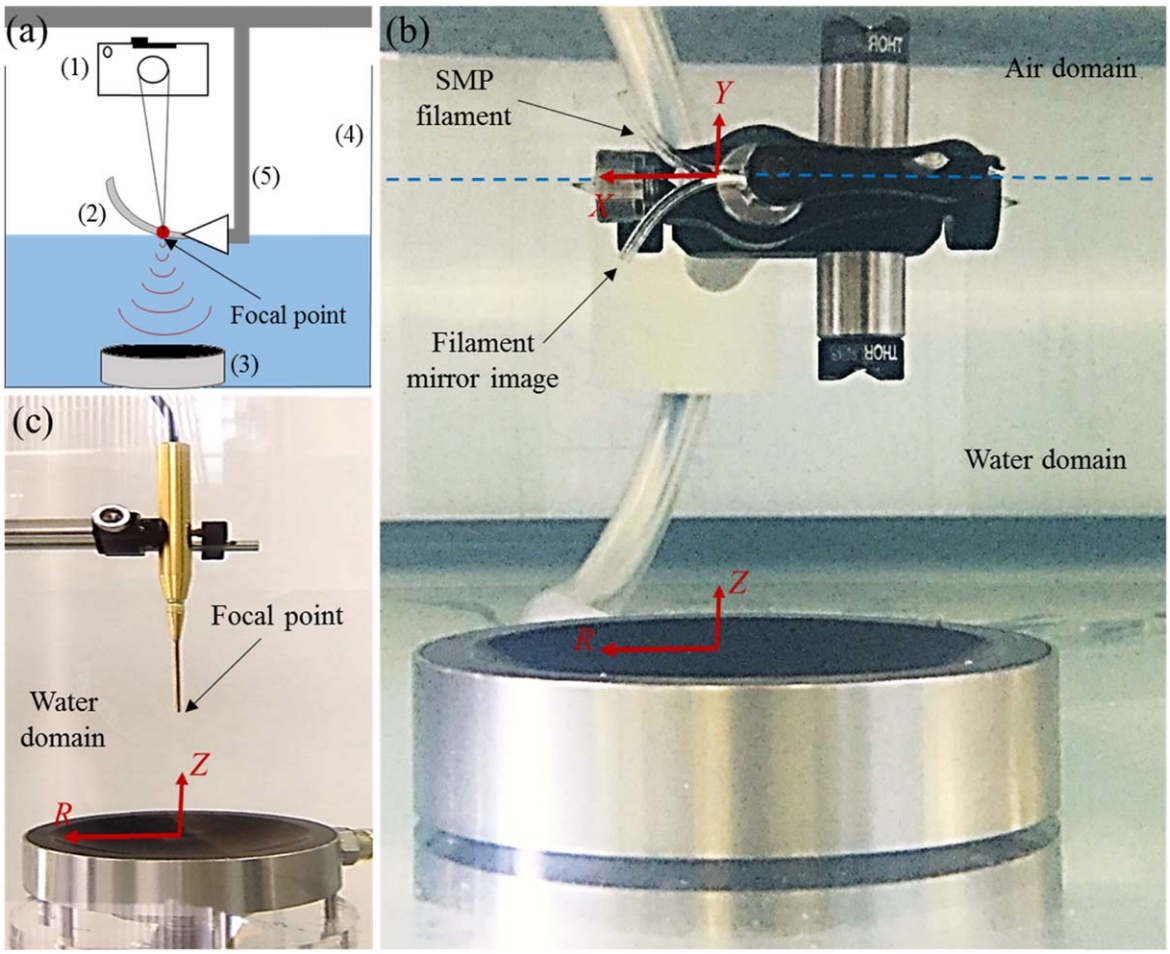

Figure 2. (a) Illustration of the experimental setup; (1) thermal imaging camera directed at the focal point, (2) SMP cantilever filament exposed to FU, (3) HIFU transducer, (4) water tank and (5) positioning system. (b) Experimental setup of an SMP filament with fixed-free boundary conditions deformed in a temporary shape. (c) Experimental setup of a needle hydrophone mounted on the positioning system and exposed to FU. The tip of the needle lies at the focal point of the transducer. *R* and *Z* are the radial and axial coordinate axis for the transducer setup, respectively.

3. Experimental results and model validation

3.1. Experimental setup and DMA tests' results

A 25 mm long, 3 mm wide and 1.5 mm thick SMP filament is used for the experimental setup in figure 2 to study FU generated thermally induced shape recovery of SMP cantilever beam. The filament composed of 95% TBA and 5% DEGMA, is exposed to harmonic acoustic pressure field generated by a H-104–4 A SONIC Concepts high intensity focused ultrasound (HIFU) transducer for 20 continuous seconds, figures 2(a) and (b). The SMP is mounted with a fixed-free boundary condition to mimic a cantilever beam using a positioning system. The water level in the tank is maintained such that the bottom part of the filament is submerged in water and the focal point of the FU transducer lies inside the submerged portion of the filament. Special care is taken to maintain the power of the transducer below a threshold level to prevent degradation of the sample [30]. A FLIR C2 infrared camera is used to capture thermal images during 20 s of ultrasound actuation with additional 20 s to capture cool down (figure 2(a)). Experiments are conducted for pressure measurement from FU transducer as shown in figure 2(c). A Precision Acoustics 1 mm needle hydrophone is used to acquire pressure measurements using NI SignalExpress® software through a National Instrument data acquisition device (PCI-6115). The hydrophone is mounted using a positioning system and measures pressure data in axial and radial directions of the transducer to capture the exact location of the focal point. The pressure measured at the focal point is then used for analysis and model validation. Figures 3(a) and (b) show the storage modulus and tan delta curves obtained from DMA tests for 95% TBA-5% DEGMA, respectively. While storage modulus gives insight into the material's elastic behavior, tan delta is a measure of energy dissipation when the material is subjected to sinusoidal force and varying temperature. A detailed explanation of the fabrication of the SMP filament, DMA tests and thermal experiments for its characterization is given in our previous work [30] as well as in the supplementary material, available online at stacks.iop.org/SMS/28/055002/mmedia. Figure 3 shows the variation of mechanical properties with temperature which forms the basis of the shape recovery response and will

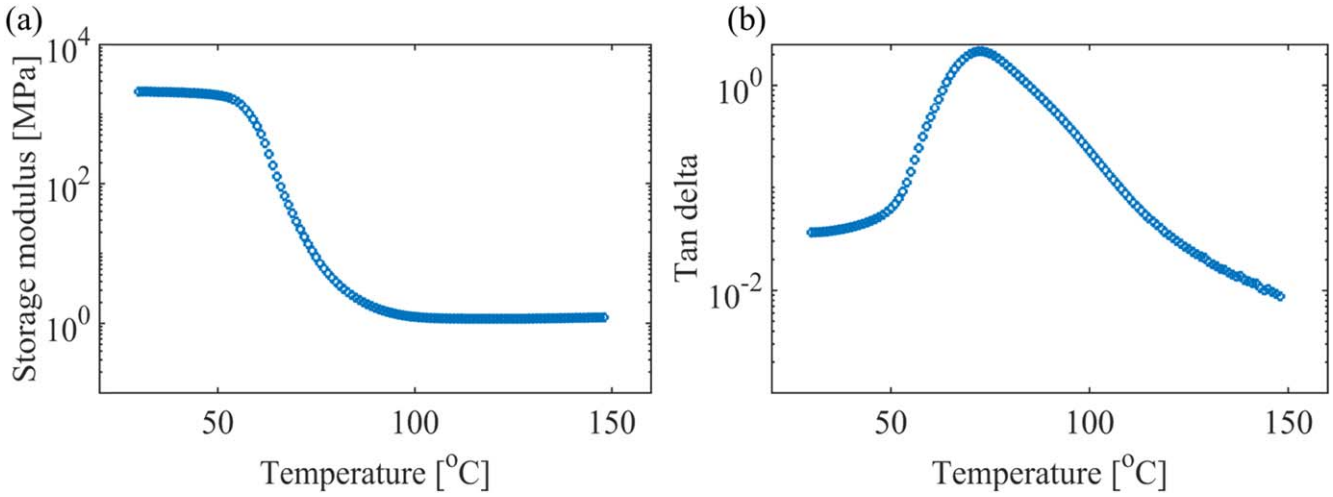

Figure 3. (a) Storage modulus and (b) tan delta obtained from DMA tests for 95% TBA-5% DEGMA composition.

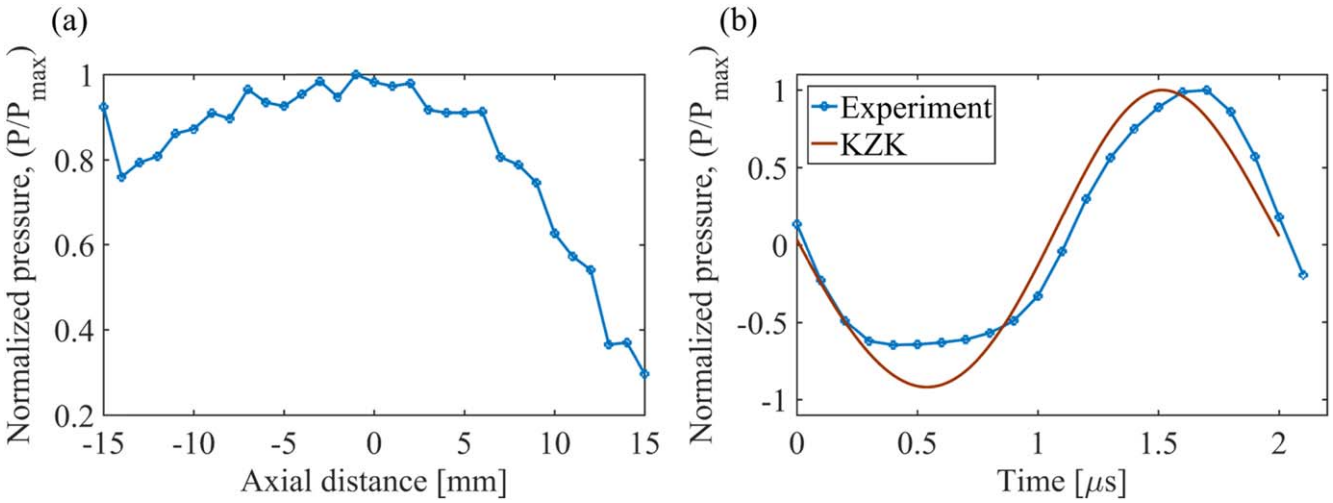

Figure 4. (a) Normalized pressure along axial axis and (b) normalized pressure waveform at focal point (0 mm) at 10 W and 0.5 MHz source frequency in water domain.

be used in our analysis, as explained in later sections. It is important to note that the heating rate shifts the transition temperature [65]. Since the actuation with FU has a varying heating rate, the transition temperature in our experiments is different from the transition temperature obtained from DMA.

3.2. Acoustic-thermal model validation

The developed analytical-numerical model [30], explained in section 2, is used to study the acoustic and thermal fields of the FU actuated cantilever beam. The thermal energy induces shape recovery behavior modelled through the constitutive equations in section 2 (equations (3), (4) and (9)). To study sound wave propagation in SMP, the model predicted acoustic field is first validated through experiments only in water domain, using hydrophone (figure 2). Figure 4(a) shows the normalized sound pressure along the axial axis measured by the hydrophone at 10 W input power and 0.5 MHz source frequency. A good agreement is observed between the waveform obtained from KZK model and experiments for the normalized pressure wave at the focal point as shown in figure 4(b). The pressure is normalized with respect to the maximum pressure at the focal point, P_{max}.

The acoustic model is now used to calculate the pressure field at the focal point inside SMP. A numerical validation of the model estimated acoustic behavior in SMP upon FU exposure, is done with finite element method in our previous work with good agreement [30]. Our previous study [42] also discusses in-depth, the influence of medium parameters such as diffraction, attenuation and nonlinearity of the medium, and input parameters such as input power and source frequency on the nonlinearity of the propagating sound wave in the SMP. It is known that an increase in the number and amplitude of the higher harmonics increases the nonlinearity and the total acoustic energy of the pressure wave at a point. Our previous study [42] observed that a higher coefficient of nonlinearity of the SMP as compared to water, increase in source frequency and input power have a nonlinearly proportional influence on the nonlinearity of the acoustic wave. It was shown that the wave

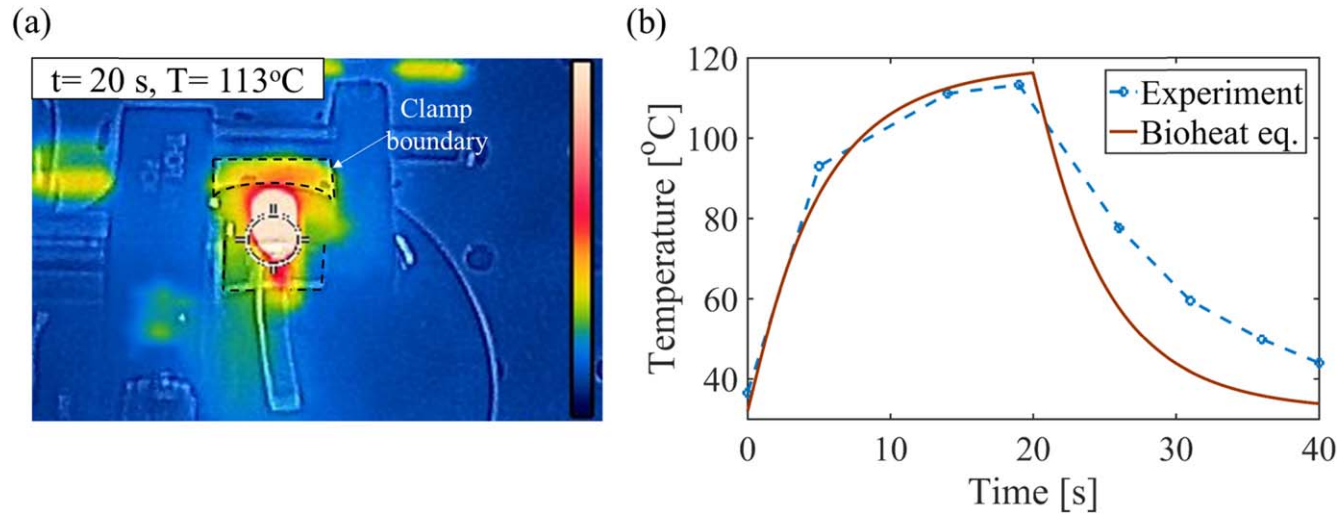

Figure 5. (a) Thermal image of SMP cantilever during ultrasound actuation at 20 s and (b) temperature rise with actuation time at the focal point in SMP.

nonlinearity is an important parameter to consider since the absorption of the acoustic energy in SMP is proportionally correlated to the energy transfer in the higher harmonics. Due to the absorption of the ultrasound waves in the polymer, a viscous shearing effect on the molecules is created which causes a release of energy in the form of heat. Therefore, it was concluded that the higher the nonlinearity of the propagating wave, the more is the absorption and an increase in the temperature of the polymer which increases the shape recovery of the SMP. Consequently, in this work, we use 10 W of input power at 0.5 MHz frequency to achieve shape recovery at a reasonable spatial scale.

Using equation (2), the absorbed pressure field in SMP predicts the temperature rise in the filament during ultrasound actuation. Figure 5(a) shows the thermal image of ultrasound actuated SMP at 20 s with 10 W input power and 0.5 MHz source frequency. The circle in the image shows the region of highest energy concentration. As can be seen, the temperature of the surrounding water is approximately at room temperature which emphasizes the localized heating effect of FU actuation. Figure 5(b) shows the corresponding temperature rise at the focal point for the experimental setup depicted in figure 2. A good agreement is observed between the temperature predicted by the model and the experiment.

To study the dynamic response of SMP during the four stages of shape recovery, it is important to account for the temperature dependent mechanical properties of SMP. Figure 3 shows the change in the stiffness of the SMP used in this study, with temperature through DMA experiments. It is seen that, at high temperatures, the stiffness of the polymer is low and the elastic deformation produces a change in the conformational entropic state of the polymer chains resulting in a ductile, rubbery behavior of the polymer. At low temperatures below glass transition temperature, $T \cong 72\ ^{\circ}\mathrm{C}$ (for SMP in this study), the polymer is in a glassy state and behaves as an elastic solid [35]. To understand the shape memory behavior, the dynamic analytical model is divided into the following four stages.

3.3. Dynamics of SMP shape recovery under focused ultrasound actuation

3.3.1. Loading, cooling and shape fixation model validation.

In the loading stage, the SMP filament (initial straight shape) is mounted with one end fixed using a clamp. The material is then heated to a temperature T_h such that it becomes amorphous. A pre-determined end-point deflection of approximately 15 mm is applied at the free end of the cantilever. The deflection is calculated from the horizontal axis, X in the vertical direction, Y. This gives an end-point vertical force of approximately 6 mN for static deflection of beam as calculated by equation (14). The deflection is maintained until the filament cools down. Figure 2(b) shows the temporary shape of the beam in this stage. Bergman *et al* [59] solved the loading stage behavior to mimic an Euler–Bernoulli beam under static loading, given by equation (14) using numerical methods. In this study, we use homotopy analysis method [61] to derive an analytical solution of equation (14) to predict the deflection of the beam. The analytical solution gives us the advantage of estimating the resulting strains, ε_{pre} which are used as a boundary condition in equation (4) by setting $\varepsilon = \varepsilon_{pre}$ to predict the frozen strains in cooling stage. Figures 6(a) and (b) show the strains developed and angular displacement of the beam respectively. Figure 6(c) shows the transverse (upward) deflection of the beam upon application of end point force at $T > T_g$.

During cooling, the external force is maintained as the temperature of the beam decreases. With lowering of temperature, the polymer becomes stiffer with increase in the elastic modulus and stores the elastic strains developed due to static loading, in the form of internal 'frozen' strains (equation (4)). It is assumed that at $T < T_g$, the complete filament transitions from amorphous to glassy state and $\phi_f = 1$. After cooling down in the fixation stage, the external forces are removed and due to high elastic modulus and stored energy, the beam remains fixed in its deformed 'fixed' position. To analytically formulate the temporary deflection

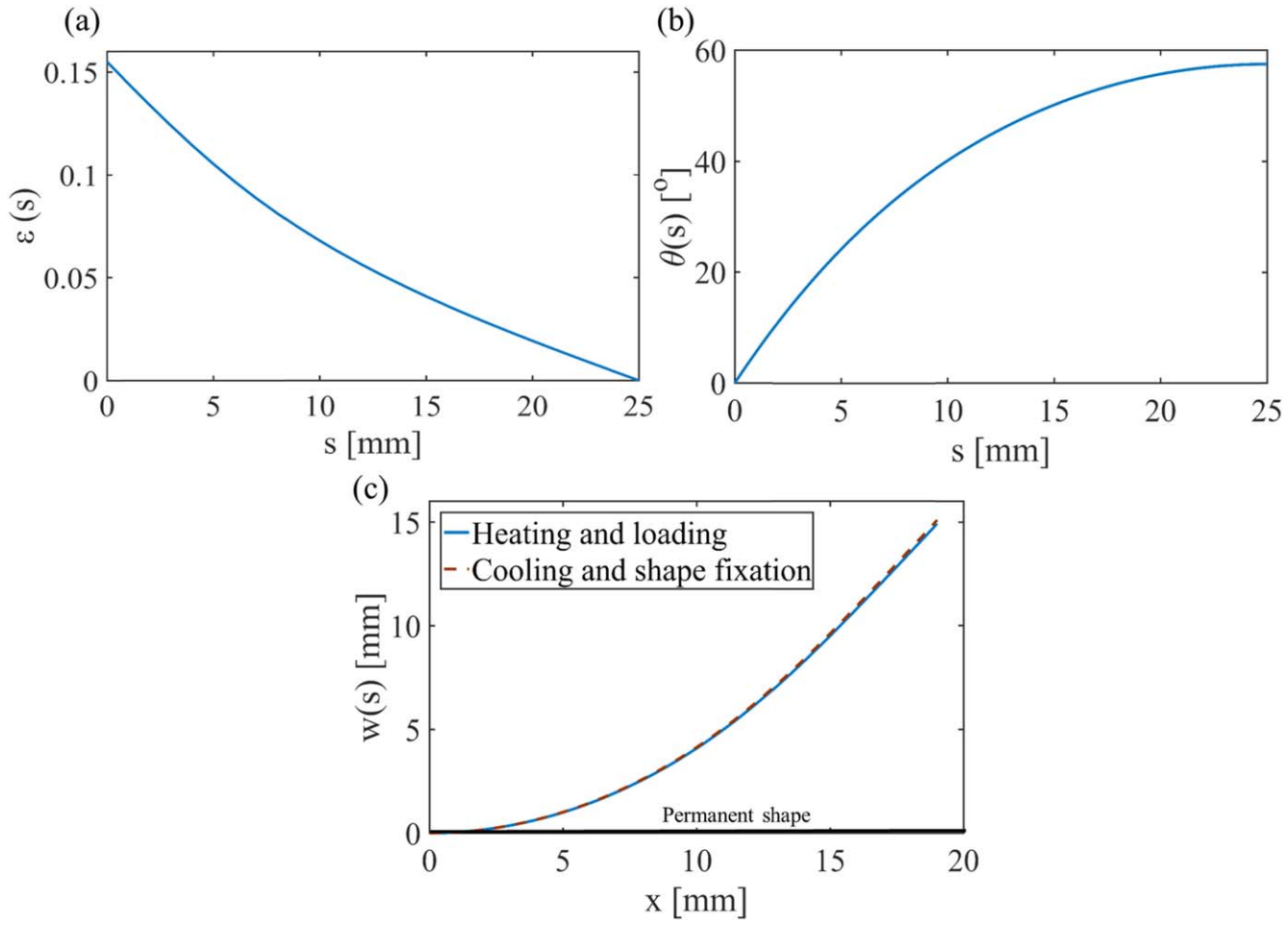

Figure 6. Static loading of cantilever beam showing (a) strain and (b) angular displacement of the beam upon loading. (c) Transverse displacement of the beam at loading stage (force applied), $T > T_g$ and at unloading (no force applied), $T < T_g$.

of the beam in the absence of external forces and account for the frozen energy, Generalized Hamilton's principle is used along with equations (4) and (9) to derive equation (16) in section 2.2.2. Figure 6(c) shows that the beam remains approximately at the same position before and after the removal of the external forces at cool down ($T < T_g$) since all the strains applied during loading are frozen. Similar observations were made during our experiments. At this stage, the beam is mounted in the experimental setup, figure 2(b), to study ultrasound induced shape recovery behavior.

3.3.2. Shape recovery model validation and the effects of peak pressure. In the shape recovery stage, ultrasound-induced thermal energy increases the temperature of the SMP filament which results in a decrease of the temperature dependent stiffness of the polymer and the polymer transitions into rubbery state. Since, the temperature rise occurs during 20 s of ultrasound actuation, it is important to formulate the changing stiffness with actuation time. As a first step, a phenomenological relation of temperature, T variation with time, t, is obtained at different peak pressures in SMP, $P_{\max}$ and source frequency, f_0, and is given by

$$T = ae^{bt} + ce^{dt}, \tag{29}$$

where parameters a, b, c and d are non-dimensional second order polynomials in $P_{\max}$ and third order polynomials in f_0, figures S1 and S2, respectively. Tables S2 and S3 list the value of the coefficients of the polynomials in f_0 and $P_{\max}$, respectively. In the second step, using equation (29) and the relation of E with temperature from DMA analysis as shown in figure 3(a) [30], an FU actuation time dependent Young's modulus is obtained as a function of $P_{\max}$ and f_0, which is used in the equation of motion for shape recovery of the SMP beam, figure S3. For FU actuation of SMPs, the heating rate is not constant and changes from high to low as the actuation time increases, figure 5(b). Many works have incorporated the effects of heating rate through a phenomenological relation by expressing frozen fraction as $\phi(T, \dot{T})$ or frozen strains as $\varepsilon_s(T, t)$ or $\varepsilon_s(T, \dot{T})$ [38, 66, 67]. However, since the FU actuation can be controlled through source power and source frequency only, instead of directly manipulating heating rate, equation (29) is formulated which captures the changing heating profile with change in $P_{\max}$ (function of source power) and f_0. This intrinsically incorporates the changing heating rate profile

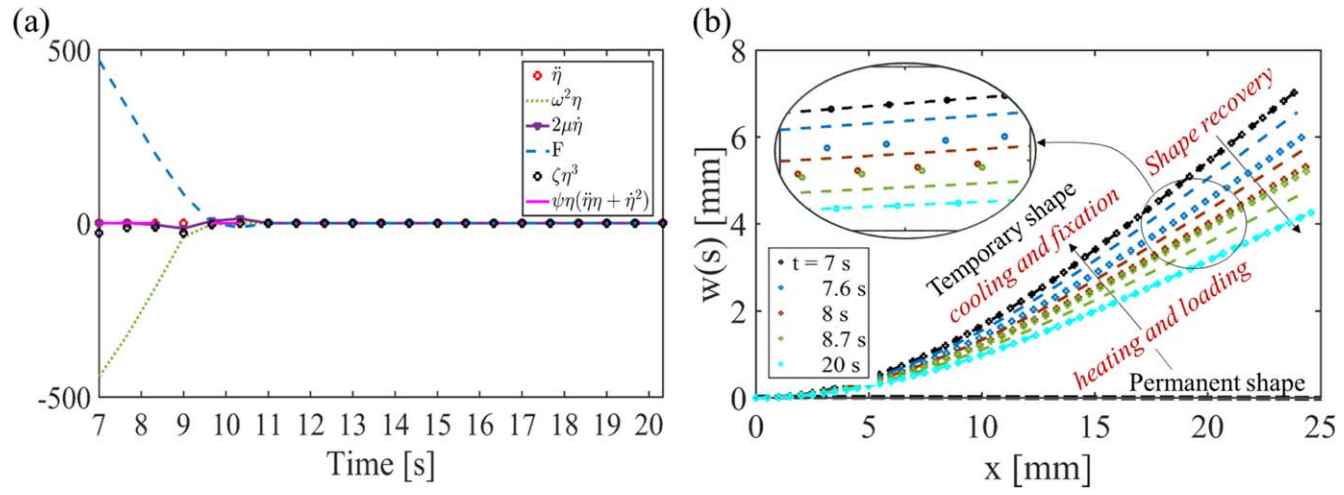

Figure 7. (a) Time history of the individual terms in equation (15) starting at the onset of the shape recovery at 7 s. Here F is the term defined in equation (21) at the corresponding time. (b) Beam deflection at various instances of time during shape recovery obtained from numerical solution of equation (15), hollow circle symbols, and method of multiple scales, dashed lines; the inset shows a magnified image where change in color represents the change in time.

Table 1. Thermomechanical properties of SMP in this study.

Parameters	Value
Modulus at $T < T_g$	1.23 MPa
Modulus at $T > T_g$	2.1 GPa
c_f	2.84×10^{-15}
n	11
N	8.04×10^{25} molecules/m^3
$\alpha(T)$	$-6.47 \times 10^{-4} + 2.35 \times 10^{-6}$ T K^{-1} [68]
T_h	373 K

which affects the release rate of temperature dependent frozen strains, since $T = T(P_{\max}, f_0, t)$ from equation (29).

To model the equation of motion of the cantilever SMP beam during shape recovery, the derivation in section 2.2.2 is used. Applying modal analysis and Galerkin's weighted residual method to distributed parameter governing equation (9), equation (15) is obtained which accounts for the time variation of material properties during ultrasound exposure. The frozen internal energy given by equation (8), releases nonlinearly with actuation time as the beam heats and recovers. A constant value of damping ratio at $T = T_g$ is considered and is obtained from the DMA analysis (figure 3). The material properties used in the analytical model are derived from experiments and are listed in table 1.

In order to derive an analytical expression for the shape recovery of the beam, method of multiple scales is applied to equation (15). However, since the method of multiple scales is limited to weak nonlinearities in the system [57], the forcing applied on the system during loading stage is small enough such that the geometric nonlinearities in equation (15) are weak. The equation is then scaled with a book-keeping parameter, $\tilde{\varepsilon}$ to obtain equation (17). Since, the internal frozen energy and the elastic modulus are changing with time, the process of shape recovery is divided into multiple stages of constant coefficients of geometric nonlinearities where the initial conditions of each stage depend on the behavior of the beam in the previous stage. For each stage accounting for a fraction of the total time, equation (17) is used to obtain the response of the beam. This iterative process is followed until the nonlinear terms become negligible (>O($\tilde{\varepsilon}$)) and the response at that stage is predicted by the linear equation (18) accurately. Figure 7(a) shows the influence of individual terms in equation (15) on the response of the beam based on which scaling is done. A validation of the method of multiple scales for weak nonlinearities is done with numerical solution of equation (15) using NSolve in Mathematica®, figure 7(b) with good agreement. It was observed that the agreement with numerical solution is good when the weakness of the geometric nonlinearities' is of the order of. 1 or smaller i.e. $\tilde{\varepsilon} \leqslant 0.1$. The maximum error between the two solutions for the transverse displacement of the free end is 8.5% and can be considered negligible for practical applications. The increasing difference between the two solutions in the intermediate time intervals in figure 7(b) is because of the change in the order of the geometric nonlinearities from $\tilde{\varepsilon}$ to $\tilde{\varepsilon}^2$. However, in this work, the solution until $O(\tilde{\varepsilon})$ is obtained. Figure 7(b) shows an approximately 20% shape recovery upon 20 s of actuation time at 10 W power and 0.5 MHz of source frequency. In order to achieve full shape recovery, repeated cycles of HIFU exposure are needed due to the slow response time of SMPs. Similar observations of repeated actuation were observed in experiments and by Lu *et al* [69]. Another reason for partial shape recovery is the geometry of the exposed SMP which plays a significant role in the temperature distribution of the exposed area [30]. Bhargava *et al* [30] observed that a sharpness of the deformed angle exposed to FU leads to higher temperature concentration and faster shape recovery.

Figure 8 shows the experimental validation of the numerical solution of equation (15) with good agreement at 10 W of input power and 0.5 MHz of source frequency. The numerical solution is used for experimental validation in order to obtain the deformation at a large spatial scale which leads to strong geometric nonlinearities in the temporary

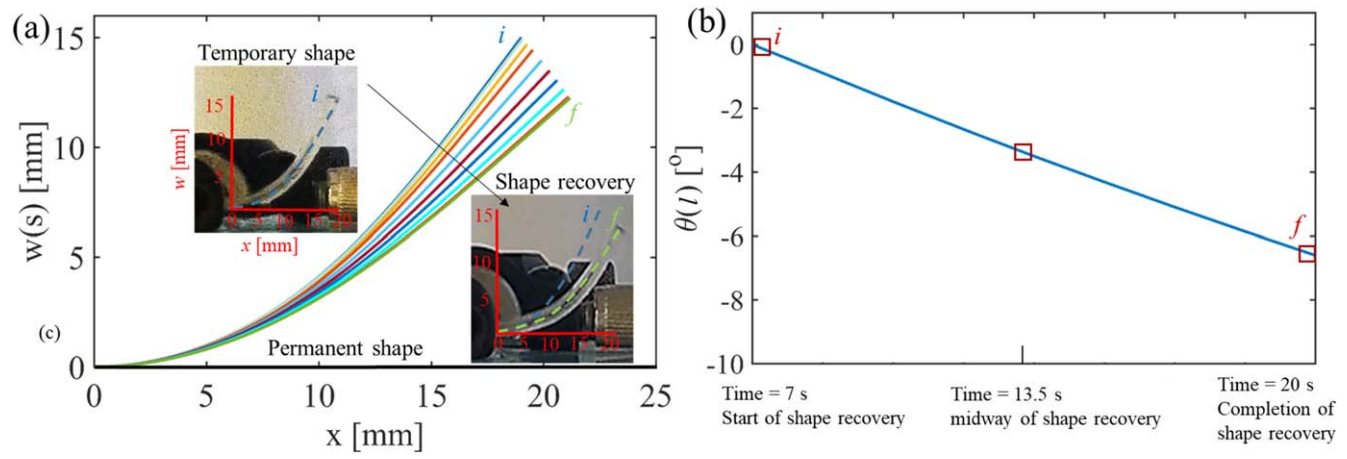

Figure 8. (a) Transverse displacement during shape recovery. The insets show the deformed shape as well as the initial and final position of the beam. (b) Time history of the deformation angle of the free end of the beam. The square markers show the experimentally observed deformation angle at the corresponding time during shape recovery. Here *i* denotes the initial angle at temporary shape and *f* denotes the final angle after shape recovery.

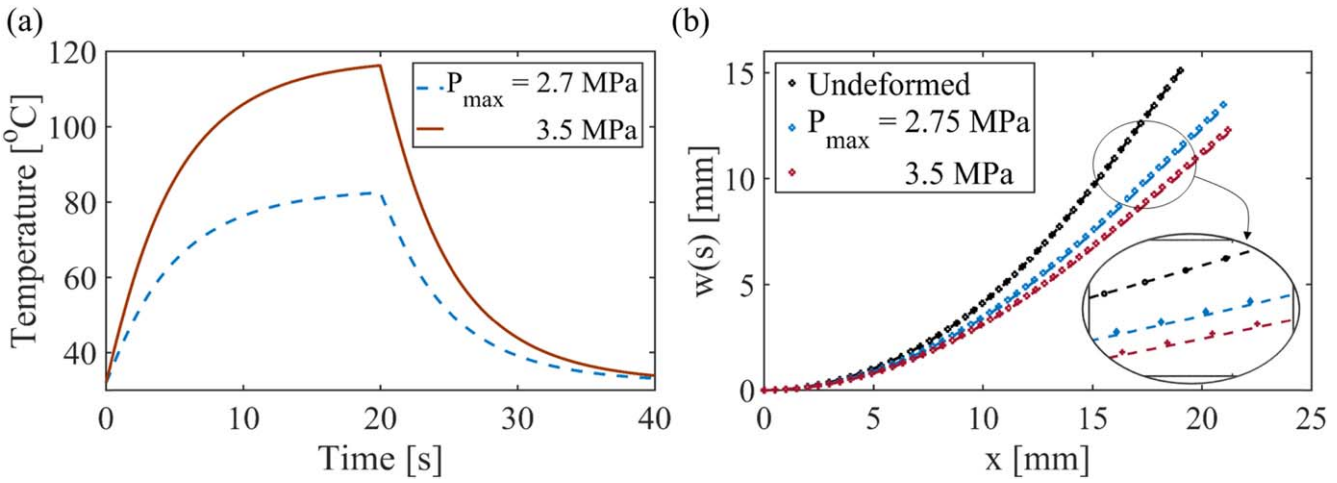

Figure 9. (a) Time history of temperature rise inside SMP at focal point and (b) transverse beam deformation from experiment (dashed) and analytical model (circular symbols) at different P_{max}; the inset shows a magnified image where change in color shows the change in P_{max}.

shape. Since method of multiple scales is only applicable for weak non-linearities, numerical solution f equation (15) is used for comparison with experiments. Figure 8(a) shows the initial and final positions of the beam obtained from model and experiments, plotted against horizontal displacement, x, calculated as $x = \int_0^s \cos[\theta(s, t)]ds$. It is noted that for the cantilever beam in this study, the recovery starts at 7 s post initiation of ultrasound exposure, figure 8(b).

To study the effect of acoustic parameters on shape recovery response using the developed analytical model, peak acoustic pressure inside the SMP, P_{max} is varied. It is observed that the strain release due to the release of internal frozen energy inside the SMP varies with variation in P_{max}. Since the release of the frozen energy is dependent on the rate and amount of temperature rise inside the SMP, the energy release and thus the resulting strain release for recovery varies with temperature rise rate and amount, which depends on P_{max} as shown in figure 9(a) (equation (2)). Figure 9(b) shows the experimental validation of the deformation of the SMP cantilever beam at 0.5 MHz obtained from analytical model at different P_{max}. It is observed that with increase in peak pressure inside SMP, the temperature at the focal point at 20 s increases, increasing the temperature dependent frozen energy release and giving more shape recovery. The shape recovery in transverse direction, w, is approximately 1.5 mm at 2.7 MPa and approximately 3 mm at 3.5 MPa.

4. Conclusions

As an alternative to relatively well-studied methods of external stimulus to trigger the shape recovery of SMPs, namely light and magnetic field, FU is used to actuate the thermal-responsive SMPs in this study. The underlying mechanism of FU actuation is that the induced thermal energy is a result of selective, localized and controllable heating by FU, which influences the mechanical behavior of SMP. FU actuation offers advantage of temporal and spatial control through flexible selection of the

acoustic intensity, frequency, exposure time, sample size as well as the ease in positioning of the acoustic source. While non-contact ultrasound triggering has been used to achieve broad utilization of SMPs, to the best of our knowledge, no report involved an analytical solution to analyze the acoustic-thermo-elastic dynamics of ultrasound-responsive SMPs. This paper presents a fundamental research focusing on ultrasound actuation of SMPs considering acoustic, mechanical and geometric nonlinearities and aims to show the dynamical behavior of SMPs during the four stages of shape recovery process. The FU induced thermal energy inside SMP causes a nonlinear change in thermomechanical properties namely elastic modulus and thermal expansion coefficient, with respect to actuation time. A model is developed which accounts for this nonlinear temporal variation of material properties and uses method of multiple scales to derive a solution of the governing equations of motion of an Euler–Bernoulli SMP cantilever beam assuming weak geometric nonlinearities. The analytical solution is successfully validated with numerical solutions and experiments. While the solution of method of multiple scales can give accurate shape recovery response for temporary deformations with weak geometric nonlinearities such as electrical switches, the semi-numerical modal analysis solution can predict shape memory behavior with strongly geometrically nonlinear temporary shapes. In both the cases, the shape recovery response is expressed as a function of acoustic and thermal parameters, thus eliminating the need of calculating any intermediary or internal acoustic/thermal/elastic effects on SMP.

Acknowledgments

This work was partially supported by the National Science Foundation Grant No. ECCS-1711139, which is gratefully acknowledged.

ORCID iDs

Shima Shahab https://orcid.org/0000-0003-1970-5345

References

[1] Ratna D and Karger-Kocsis J 2008 Recent advances in shape memory polymers and composites: a review *J. Mater. Sci.* **43** 254–69

[2] Zarek M, Layani M, Cooperstein I, Sachyani E, Cohn D and Magdassi S 2016 3D printing of shape memory polymers for flexible electronic devices *Adv. Mater.* **28** 4449–54

[3] Dietsch B and Tong T 2007 A review-: features and benefits of shape memory polymers (smps) *J. Adv. Mater.* **39** 3–12

[4] Liu C, Qin H and Mather P 2007 Review of progress in shape-memory polymers *J. Mater. Chem.* **17** 1543–58

[5] Metcalfe A, Desfaits A-C, Salazkin I, Yahia L H, Sokolowski W M and Raymond J 2003 Cold hibernated elastic memory foams for endovascular interventions *Biomaterials* **24** 491–7

[6] Sharp A A, Panchawagh H V, Ortega A, Artale R, Richardson-Burns S, Finch D S, Gall K, Mahajan R L and Restrepo D 2006 Toward a self-deploying shape memory polymer neuronal electrode *J. Neural Eng.* **3** L23

[7] Small W, Metzger M F, Wilson T S and Maitland D J 2005 Laser-activated shape memory polymer microactuator for thrombus removal following ischemic stroke: preliminary *in vitro* analysis *IEEE J. Sel. Top. Quantum Electron.* **11** 892–901

[8] Maitland D J, Metzger M F, Schumann D, Lee A and Wilson T S 2002 Photothermal properties of shape memory polymer micro-actuators for treating stroke *Lasers Surg. Med.* **30** 1–11

[9] Yakacki C M, Shandas R, Lanning C, Rech B, Eckstein A and Gall K 2007 Unconstrained recovery characterization of shape-memory polymer networks for cardiovascular applications *Biomaterials* **28** 2255–63

[10] Lendlein A and Langer R 2002 Biodegradable, elastic shape-memory polymers for potential biomedical applications *Science* **296** 1673–6

[11] Mather P T, Luo X and Rousseau I A 2009 Shape memory polymer research *Annu. Rev. Mater. Res.* **39** 445–71

[12] Amamoto Y, Otsuka H, Takahara A and Matyjaszewski K 2012 Self-healing of covalently cross-linked polymers by reshuffling thiuram disulfide moieties in air under visible light *Adv. Mater.* **24** 3975–80

[13] Ghosh B and Urban M W 2009 Self-repairing oxetane-substituted chitosan polyurethane networks *Science* **323** 1458–60

[14] Fang L, Fang T, Fang Z, Lu C and Xu Z 2016 Solar light responsive polymer composites with three shape-memory effects *Macromol. Mater. Eng.* **301** 267–73

[15] Meng H and Li G 2013 A review of stimuli-responsive shape memory polymer composites *Polymer* **54** 2199–221

[16] Hribar K C, Metter R B and Burdick J A 2009 Novel nano-composite biomaterials that respond to light *Engineering in Medicine and Biology Society, 2009. EMBC 2009. Annual Int. Conf. IEEE*

[17] Bai Y, Zhang J and Chen X 2018 A thermal-, water-, and near-infrared light-induced shape memory composite based on polyvinyl alcohol and polyaniline fibers *ACS Appl. Mater. Interfaces* **10** 14017–25

[18] Chen M-C, Tsai H-W, Chang Y, Lai W-Y, Mi F-L, Liu C-T, Wong H-S and Sung H-W 2007 Rapidly self-expandable polymeric stents with a shape-memory property *Biomacromolecules* **8** 2774–80

[19] Small W, Buckley P R, Wilson T S, Benett W J, Hartman J, Saloner D and Maitland D J 2007 Shape memory polymer stent with expandable foam: a new concept for endovascular embolization of fusiform aneurysms *IEEE Trans. Biomed. Eng.* **54** 1157–60

[20] Sahoo N G, Jung Y C, Goo N S and Cho J W 2005 Conducting shape memory polyurethane-Polypyrrole composites for an electroactive actuator *Macromol. Mater. Eng.* **290** 1049–55

[21] Sahoo N G, Jung Y C and Cho J W 2007 Electroactive shape memory effect of polyurethane composites filled with carbon nanotubes and conducting polymer *Mater. Manuf. Processes* **22** 419–23

[22] Yu X, Zhou S, Zheng X, Guo T, Xiao Y and Song B 2009 A biodegradable shape-memory nanocomposite with excellent magnetism sensitivity *Nanotechnology* **20** 235702

[23] Kumar U N, Kratz K, Behl M and Lendlein A 2012 Shape-memory properties of magnetically active triple-shape nanocomposites based on a grafted polymer network with two crystallizable switching segments *Express Polym. Lett.* **6** 26–40

[24] Cuevas J, Alonso J, German L, Iturrondobeitia M, Laza J, Vilas J and León L 2009 Magneto-active shape memory composites by incorporating ferromagnetic microparticles in a thermo-responsive polyalkenamer *Smart Mater. Struct.* **18** 075003

[25] Razzaq M Y, Anhalt M, Frormann L and Weidenfeller B 2007 Thermal, electrical and magnetic studies of magnetite filled polyurethane shape memory polymers *Mater. Sci. Eng.* A **444** 227–35

[26] Kost J, Leong K and Langer R 1989 Ultrasound-enhanced polymer degradation and release of incorporated substances *Proc. Natl Acad. Sci.* **86** 7663–6
[27] De Geest B G, Skirtach A G, Mamedov A A, Antipov A A, Kotov N A, De Smedt S C and Sukhorukov G B 2007 Ultrasound-Triggered release from multilayered capsules *Small* **3** 804–8
[28] Husseini G A, Rapoport N Y, Christensen D A, Pruitt J D and Pitt W G 2002 Kinetics of ultrasonic release of doxorubicin from pluronic P105 micelles *Colloids Surf.* B **24** 253–64
[29] Bhargava A, Peng K, Mirzaeifar R and Shahab S 2018 Ultrasound actuated shape-memory polymer based drug delivery containers *Proc. SPIE* **10595** 105952H
[30] Bhargava A, Peng K, Stieg J, Mirzaeifar R and Shahab S 2017 Focused ultrasound actuation of shape memory polymers; acoustic-thermoelastic modeling and testing *RSC Adv.* **7** 45452–69
[31] Tobushi H, Hashimoto T, Hayashi S and Yamada E 1997 Thermomechanical constitutive modeling in shape memory polymer of polyurethane series *J. Intell. Mater. Syst. Struct.* **8** 711–8
[32] Tobushi H, Okumura K, Hayashi S and Ito N 2001 Thermomechanical constitutive model of shape memory polymer *Mech. Mater.* **33** 545–54
[33] Morshedian J, Khonakdar H A and Rasouli S 2005 Modeling of shape memory induction and recovery in heat-shrinkable polymers *Macromol. Theory Simul.* **14** 428–34
[34] Li Y, Guo S-S, He Y and Liu Z 2015 A simplified constitutive model for predicting shape memory polymers deformation behavior *Int. J. Comput. Mater. Sci. Eng.* **4** 1550001
[35] Liu Y, Gall K, Dunn M L, Greenberg A R and Diani J 2006 Thermomechanics of shape memory polymers: uniaxial experiments and constitutive modeling *Int. J. Plast.* **22** 279–313
[36] Qi H J, Nguyen T D, Castro F, Yakacki C M and Shandas R 2008 Finite deformation thermo-mechanical behavior of thermally induced shape memory polymers *J. Mech. Phys. Solids* **56** 1730–51
[37] Rajagopal K and Srinivasa A 1998 Mechanics of the inelastic behavior of materials—Part 1, theoretical underpinnings *Int. J. Plast.* **14** 945–67
[38] Li Y, Hu J and Liu Z 2017 A constitutive model of shape memory polymers based on glass transition and the concept of frozen strain release rate *Int. J. Solids Struct.* **124** 252–63
[39] Rozanova-Pierrat A 2006 Mathematical analysis of Khokhlov–Zabolotskaya–Kuznetsov (KZK) equationhal-00112147
[40] Hamilton M F and Blackstock D T 1998 *Nonlinear Acoustics* (San Diego: Academic)
[41] Curra F P, Mourad P D, Khokhlova V A, Cleveland R O and Crum L A 2000 Numerical simulations of heating patterns and tissue temperature response due to high-intensity focused ultrasound *IEEE Trans. Ultrason. Ferroelectr. Freq. Control* **47** 1077–89
[42] Bhargava A, Peng K, Stieg J, Mirzaeifar R and Shahab S 2017 Ultrasound actuation of shape-memory polymer filaments: acoustic-thermoelastic modeling and testing *Smart Materials, Adaptive Structures and Intelligent Systems* 2 *(Utah, Sept. 18-20, 2017978-0-7918-5826-4)*
[43] Rao S S 2007 *Vibration of Continuous Systems* (New York: Wiley)
[44] Nayfeh A H 2011 *Introduction to Perturbation Techniques* (New York: Wiley)
[45] Shahab S, Gray M and Erturk A 2015 Ultrasonic power transfer from a spherical acoustic wave source to a free-free piezoelectric receiver: modeling and experiment *J. Appl. Phys.* **117** 104903
[46] Shahab S and Erturk A 2014 Contactless ultrasonic energy transfer for wireless systems: acoustic-piezoelectric structure interaction modeling and performance enhancement *Smart Mater. Struct.* **23** 125032
[47] Bakhtiari-Nejad M, Elnahhas A, Hajj M R and Shahab S 2018 Passive metamaterial-based acoustic holograms in ultrasound energy transfer systems *Proc. SPIE* **10595** 1059518
[48] Meesala V C, Hajj M R and Shahab S 2018 Modeling electroelastic nonlinearities in ultrasound acoustic energy transfer systems *Proc. SPIE* **10595** 105951G
[49] Chen Y-C and Lagoudas D C 2008 A constitutive theory for shape memory polymers: I. large deformations *J. Mech. Phys. Solids* **56** 1752–65
[50] Chen Y-C and Lagoudas D C 2008 A constitutive theory for shape memory polymers: II. a linearized model for small deformations *J. Mech. Phys. Solids* **56** 1766–78
[51] Boyce M C and Arruda E M 2000 Constitutive models of rubber elasticity: a review *Rubber Chem. Technol.* **73** 504–23
[52] Dupaix R B and Boyce M C 2007 Constitutive modeling of the finite strain behavior of amorphous polymers in and above the glass transition *Mech. Mater.* **39** 39–52
[53] Buckley C and Jones D 1995 Glass-rubber constitutive model for amorphous polymers near the glass transition *Polymer* **36** 3301–12
[54] Buckley C, Jones D and Jones D 1996 Hot-drawing of poly (ethylene terephthalate) under biaxial stress: application of a three-dimensional glass—rubber constitutive model *Polymer* **37** 2403–14
[55] Ward I 1984 The role of molecular networks and thermally activated processes in the deformation behavior of polymers *Polymer Eng. Sci.* **24** 724–36
[56] Treloar L R G 1975 *The Physics of Rubber Elasticity* (Oxford: Oxford University Press)
[57] Nayfeh A H and Pai P F 2008 *Linear and Nonlinear Structural Mechanics* (New York: Wiley)
[58] Tang D, Zhao M and Dowell E H 2014 Inextensible beam and plate theory: computational analysis and comparison with experiment *J. Appl. Mech.* **81** 061009
[59] Bergman D, Yang B and Fang H 2013 Curvilinear quasi-static model for analysis of a shape memory polymer cantilever beam for space applications *The 14th AIAA Gossamer Spacecraft Forum (Boston)* (https://doi.org/10.2514/6.2013-1868)
[60] Gere J M and Timoshenko S P 1997 *Mech. Mater* (Boston: PWS Publishing Company)
[61] Wang J, Chen J-K and Liao S 2008 An explicit solution of the large deformation of a cantilever beam under point load at the free tip *J. Comput. Appl. Math.* **212** 320–30
[62] Meirovitch L and Parker R 2001 Fundamentals of vibrations *Appl. Mech. Rev.* **54** B100
[63] Nayfeh A H and Mook D T 2008 *Nonlinear Oscillations* (New York: Wiley)
[64] Meesala V C and Hajj M R 2018 Identification of nonlinear piezoelectric coefficients *J. Appl. Phys.* **124** 065112
[65] Yu K and Qi H J 2014 Temperature memory effect in amorphous shape memory polymers *Soft Matter* **10** 9423–32
[66] Yang Q and Li G 2016 Temperature and rate dependent thermomechanical modeling of shape memory polymers with physics based phase evolution law *Int. J. Plast.* **80** 168–86
[67] Baghani M, Naghdabadi R, Arghavani J and Sohrabpour S 2012 A thermodynamically-consistent 3D constitutive model for shape memory polymers *Int. J. Plast.* **35** 13–30
[68] Yuan C, Ding Z, Wang T, Dunn M L and Qi H J 2017 Shape forming by thermal expansion mismatch and shape memory locking in polymer/elastomer laminates *Smart Mater. Struct.* **26** 105027
[69] Lu X, Fei G, Xia H and Zhao Y 2014 Ultrasound healableshape memory dynamic polymers *J. Mater. Chem* A **2** 16051–60